The effect of reduction temperature of graphene oxide on the structure and

properties of polystyrene/thermally reduced graphene oxide

nanocomposites

Zaid G. Mohammadsalih^{a, b}, Beverley J. Inkson^c and Bigiong Chen d,*

^a Applied Science Research Unit, College of Applied Science, University of Technology- Iraq.

^bAdvanced Engineering Materials and Composites Research Centre (AEMC), Department of Mechanical and

Manufacturing Engineering, Universiti Putra Malaysia, 43400 UPM Serdang, Selangor, Malaysia.

^c Department of Materials, University of Sheffield, Mappin Street, Sheffield, S1 4NS, United Kingdom.

d School of Mechanical and Aerospace Engineering, Queen's University Belfast, Stranmillis Road, Belfast, BT9 5AH,

United Kingdom.

*Corresponding Author Email Address: b.chen@qub.ac.uk

Abstract

The adoption of an eco-friendly approach to reduce graphene oxide (GO) and the employment of the obtained reduced graphene oxide (rGO) to prepare high-performance polymer nanocomposites represent a considerable

challenge. Vacuum assisted low temperatures were used to obtain rGO from GO. GO was reduced at 130, 165

and 200 °C for 24 h to produce rGOs of different degrees of reduction. Fourier infrared spectroscopy (FTIR), X-

ray diffraction (XRD), Raman spectroscopy, thermogravimetric analysis (TGA) and X-ray photoelectron

spectroscopy confirmed a successful reduction of GO and the preparation of rGOs with different degrees of

reduction. To study the effect of rGOs on the structure and properties of polymers, rGOs were mixed with

polystyrene (PS) at 1.0 wt. % loading to prepare nanocomposites using a solution blending method. The results

of FTIR, XRD, and scanning electron microscopy showed a possible interaction and good dispersion of GO and

its reduced forms within the host medium of PS. Differential scanning calorimetry, TGA, and dynamic mechanical

analysis showed that thermal and thermomechanical behaviour were improved with the incorporation of rGOs as

compared with nanocomposite reinforced with pristine GO and the neat polymer. The higher values of thermal

degradation temperature, glass transition temperature and storage modulus for PS/rGOs as compared with PS/GO

and the neat polymer confirmed the role of rGO in achieving better performance for the nanocomposites.

Keywords: Polystyrene, reduced graphene oxide, structure, properties.

1

1. Introduction

Graphene, a two-dimensional carbonaceous material derived from graphite, is a planar monolayer with a two-dimensional hexagonal honeycomb lattice [1]. Since its discovery, graphene has become a promising candidate in a wide array of potential applications ranging from electronics to nanocomposites due to its remarkable thermal, electrical and mechanical properties and the possibility of being incorporated as a nanofiller in polymer matrices [2, 3].

To realize the full potential applications of graphene, technologies to produce graphene at large scale are required. Many approaches have been adopted during recent years such as micromechanical cleavage, chemical vapour deposition, epitaxial growth, chemical reduction and thermal reduction of graphene oxide GO [4]. The nanosheets of GO can be prepared by oxidation of graphite using strong oxidizers. The oxidation process is of low cost and can be readily scaled up. Therefore, GO is a single atomic layered material that includes a range of oxygen functional groups both on its periphery and in the basal plane. It is amphiphilic and compatible with polar and non-polar polymers. The high surface area is an advantageous feature for both GO and its reduced form [5]. Removal of all or part of the oxygen functional groups from GO, which is known as reduction, has emerged as a powerful platform for obtaining graphene like materials, namely reduced graphene oxide (rGO), which restores all or part of the properties of pristine graphene [6].

Many routes of reduction, including chemical and thermal methods, have been used to obtain rGO [7]. The reduction process increases the ratio of carbon to oxygen (C: O) with an associated increase in hydrophobicity [8]. Some researchers [9, 10] studied the reduction of GO using sodium borohydride and hydrazine respectively as chemically reduction agents. Other kinds of chemical reductants, which could compete with hydrazine, include sulphur-containing compounds [11]. However, there is a growing body of literature concerning the thermal approach for reducing GO. Reducing time and temperature are the most important actions associated with the preparation of thermally rGOs (TRGOs) for the enhancement of polymer matrices [12, 13]. For instance, a previous study [14] reported the effective reinforcement of polymethyl methacrylate (PMMA) nanocomposites using TRGO. Hot pressing at 200 °C was used to obtain in situ thermal reduction for GO nano-sheets. The results showed a clear improvement in mechanical, viscoelastic and thermal properties of PMMA.

Melt mixing was employed by many researchers [15] to prepare the nanocomposites of polystyrene (PS) with TRGOs reduced at 200, 500 and 800 °C, respectively. The storage modulus and flame-retardant performance were significantly improved for the nanocomposites containing TRGOs reduced at 500 and 800 °C.

Microwave assisted exfoliation is another thermal approach that was investigated by a research group [16]. The obtained rGO via this approach was named as microwave exfoliated reduced graphene oxide (MERGO) with residual functional groups on the sheet surface. These functional groups provide fair dispersion of rGO in the matrix as well as a possible chemical bonding between the polymer matrix and graphene. For these reasons, the aforementioned researchers used MERGO to reinforce epoxy and found that tensile and flexural moduli as well as the fracture toughness were improved with the incorporation of low loadings of MERGO in the epoxy matrix. In addition, microwaves were used to induce thermal reduction of GO in aqueous media. A research group [13] used a mixed solution of N, N-dimethylacetamide and water as a medium for producing rGO under heating at 165 °C. The produced suspension was stable for many months at room temperature and the conductivity of the graphene paper produced from this rGO was considerably higher than that of GO paper. To avoid the harmful effect of reduction by chemicals and reduce energy consumption by using high temperatures, vacuum-assisted thermal reduction was used to reduce GO in a vacuum oven at lower temperatures. A previous study [17] reported the employment of 135, 165 and 1050 °C to obtain rGO with the assistance of vacuum oven. The obtained rGO was mixed with PMMA using solution blending and the resultant nanocomposites were hot-pressed at 200 °C. The conductivity increased with the incorporation of rGO in the matrix and recorded at 0.3 S cm⁻¹ for the nanocomposites blended with rGO obtained by applying 1050 °C. The conductivity for the other samples of PMMA blended with rGOs obtained at 135 and 145 °C showed low values of 6.0 x 10⁻³ and 0.1 S m⁻¹, respectively. This work aims to investigate the effects of rGO and the reduction degree of rGO on the structure and properties of polystyrene/rGO nanocomposites. Three different very low temperatures, 130 °C, 165 °C and 200 °C, were studied for the reduction of GO in a vacuum oven for energy saving, in comparison with the standard GO reduction processes employing high temperatures (e.g., ≥1000 °C) [17]. The selection of PS in this work was due to its low cost and wide variety of applications such as construction, decoration, packaging, and household. PS also has good mechanical properties, processing easiness and water resistance [18, 19]. The structure and morphologies of the rGOs reduced at different temperatures were characterized, along with the structure, thermal, and thermomechanical behaviour of PS/rGO nanocomposites, using a range of techniques.

2. Materials

PS pellets (Styron 634, Dow Chemicals) were obtained from RESINEX, UK. The following chemicals were from Sigma-Aldrich UK: graphite powder ($\leq 20 \mu m$), sulphuric acid (95 – 98%), potassium permanganate (97%), sodium nitrate (>99%), hydrochloric acid (36.5% in water), hydrogen peroxide (29 – 32% in H₂O), and tetrahydrofuran (THF, >99.5%). All the materials were used as received.

2.1. Preparation of rGOs

Graphite oxide was prepared according to a reported protocol [20], and freeze-dried GO powder was obtained according to a previously published method [21]. Three rGOs of different reduction degrees were prepared under different heat treatments. Briefly, 0.2 g of GO powder was placed inside a loosely tighten flask and heated in a vacuum oven for 24 h under 0.1 mPa at 130, 165 or 200 °C. After 24 h of heat treatment, the reduced materials rGO130, rGO165 and rGO200 were obtained as a dark black fluffy powder with an apparent volume expansion compared to GO.

2.2. Preparation of PS/rGO nanocomposites

The nanocomposites samples were prepared using THF as the solvent. 20 g of PS pellets were dissolved in 200 ml of THF using magnetic stirring for 2.0 h at 600 rpm. 0.2 g of GO and rGOs were separately suspended in 200 ml of THF, which was stirred for 2 h at 600 rpm and sonicated for 30 min. Then, the GO/THF or rGO/THF suspensions were added to the PS/THF solution. The mass fraction for GO and rGOs in PS was 1.0 wt. %, and all of the mixed suspensions were stirred for 1.5 h. 0.5 h of bath sonication using a water bath sonicator and 1.0 h of shear mixing (Silverson, UK) at 1600 rpm were then applied. The obtained suspensions of PS/GO and PS/rGOs were poured into covered glass Petri-dishes for slow evaporation of the solvent to ensure the formation of flat and smooth polymer nanocomposite films. All samples were left in a fume cupboard at ambient temperature for a week and then in vacuum oven for 36 h at 50°C to be fully dried.

2.3. Characterization

Fourier transform infrared spectroscopy (FTIR, Spectrum 100 Perkin Elmer, USA) with the range of 400 – 4000 cm⁻¹ was used for characterizing GO, rGOs, the neat polymer, and PS nanocomposites at a resolution of 4.0 cm⁻¹. The scan number was 16, and the scan speed was 0.2 cm s⁻¹. X-ray diffraction (XRD, Bruker, and D2 Phaser) was employed with a Ni filter and Cu K $_{\alpha}$ radiation. The size of the slit was 1.0 mm, with an operating current 10 mA, operating voltage 30 kV, scanning range 20 of 5° to 50°, step size 0.012°, and scanning time 0.3 s for each step.

XRD was used to characterize GO, rGOs, the neat polymer, and PS nanocomposites. Raman spectra were recorded for GO and rGOs on a Reinshaw in Via Raman microscope (England) using a 514.5 nm argon-ion laser.

Thermogravimetric Analysis (TGA, Pyris 1, Perkin Elmer, USA) was used to measure thermal degradation behaviour for GO, rGOs and nanocomposites. The TGA used N₂ atmosphere, a heating rate of 10 °C min⁻¹, and a range of test temperatures from 28 to 600 °C. For testing the quality of dispersion of GO in PS, transmission electron microscopy (TEM, FEI Tecnai) was performed for the sample of PS/GO 1.0 wt. % using an accelerating voltage of 100 kV. Ultrathin sections of 90-100 nm for the aforementioned samples were obtained using a cryo ultra-microtome (Leica Gmbh, Vienna, Austria). Cryogenic fracture surfaces were obtained via snapping samples in liquid nitrogen. Fractured samples were coated manually with silver dag before coating them with gold using a sputter coater (Emscope SC500, England). Scanning electron microscopy (SEM, Inspect F, Poland) was used to characterize the fracture surface for the samples with an accelerating voltage of 3.0 kV.

Differential Scanning Calorimetry (DSC, DSC 6, Perkin Elmer, USA) was used to measure glass transition temperature (T_g) of the polymer and nanocomposites. The mass of samples used in this experiment was 10 mg. The temperature was ramped from 25 °C to 240 °C at a heating rate of 10 °C min⁻¹, and nitrogen gas purging was used at a rate of 50 ml min⁻¹. Two heating-cooling cycles were performed on each sample, and T_g was measured from the middle point of the 2^{nd} heating run to remove any thermal history.

To confirm the presence of functional groups, and to highlight the change in the atomic ratio of carbon to oxygen for graphite, GO and rGOs, X-ray photoelectron spectroscopy (XPS) was carried out on a Kratos Ultra instrument using focused mono-chromatized Al K_{α} radiation (1486.6 eV). The samples were prepared by placing a small amount of powder into soft indium foil, which had been previously adhered to a sample holder using double sided carbon tape. Survey scans were collected between 1200 to 0 eV binding energy, at 160 eV pass energy and 1.0 eV intervals. In addition, high-resolution C 1s, O 1s, and N 1s spectra were collected over an appropriate energy range at 20 eV pass energy and 0.1 eV intervals.

The analysis area was 700 μ m by 300 μ m. The data collected was calibrated in intensity using a transmission function characteristic of the instrument (determined using software from the National Physical Laboratory, NPL) to make the values instrument independent, and data was quantified using theoretical Scofield relative sensitivity factors. The binding energy data was calibrated by making the main carbon peak C 1s at 285.0 eV.

Dynamic mechanical analysis (DMA, Perkin Elmer, DMA 8000, USA) was used to study the thermomechanical behaviour of the neat polymer and nanocomposites, using 0.1% strain, temperature range 40-130 °C, heating rate 3.0 °C min⁻¹, and oscillatory frequency 1.0 Hz. The used geometry was a single cantilever.

3. Results and discussion

3.1. rGOs

Theoretical calculations showed that the maximum pressure that needed to overcome van der Waals forces that bind graphene nano-sheets together is about 7.2 MPa [17]. To obtain the required exfoliation of GO nano-sheets under the influence of atmospheric pressure, the expansion force accompanying the thermal decomposition of GO must be higher than van der Waals forces between nano-sheets and higher than the atmospheric pressure. Vacuum plays a major role as it makes the exfoliation of GO easier [17]. The FTIR spectra for GO and the rGOs thermally reduced in vacuum are shown in figure 1. In the spectrum of GO, the peak at 1387 cm⁻¹ originates from the O-H deformation in the C-OH group, and the peak at 1224 cm⁻¹ represents the C-OH stretching vibration. The other peaks associated with GO were reported previously in the literature [21].

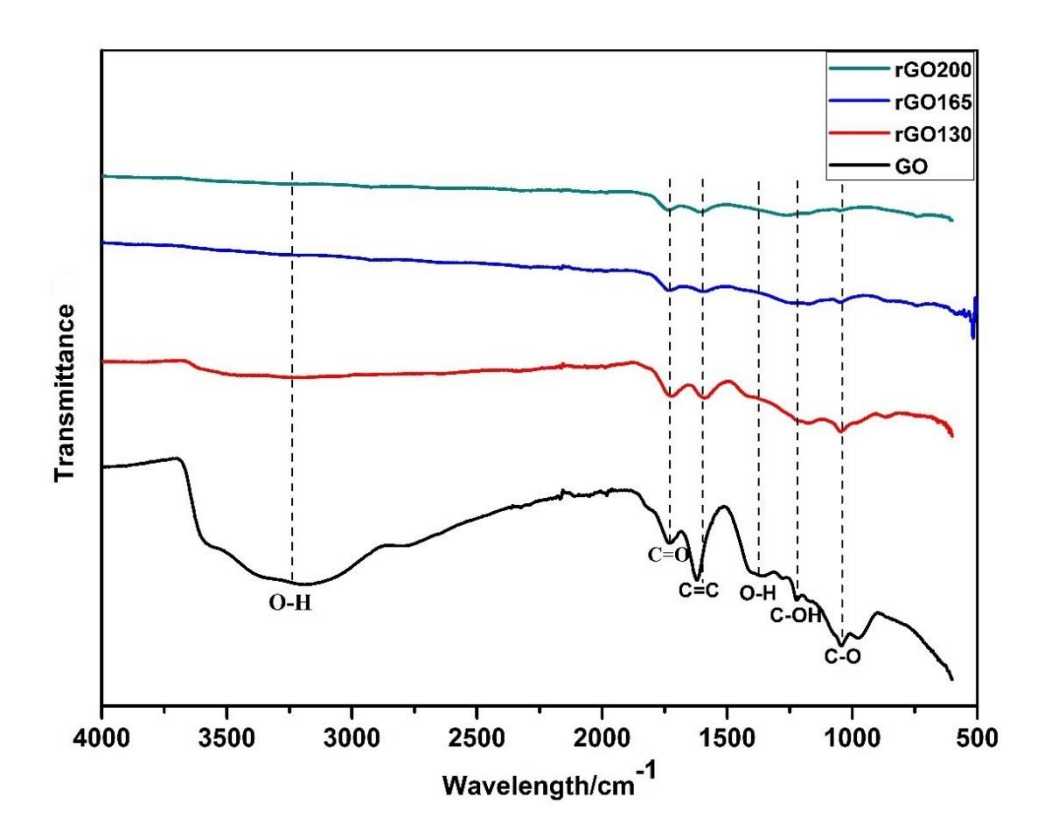


Fig. 1 FTIR spectra for GO and rGOs reduced under different temperatures in a vacuum oven. The dash lines refer to the GO functional groups which have been reduced. Spectra have been shifted vertically for clarity

A significant decrease in intensity of the peaks for the oxygenated functional groups of GO is witnessed after the thermal reduction. The peak at 3200 cm⁻¹ associated with hydroxyl groups of GO reduced its intensity for the rGO reduced at 130 °C and it totally disappeared for the rGOs reduced at 165 and 200 °C. Other peaks of GO, at 1600 cm⁻¹ related to unoxidized graphitic domain, 1720 cm⁻¹ attributed to carbonyl and carboxylic acid group, 1220 cm⁻¹ related to C-O group, and 1042 cm⁻¹ related to epoxy group, became weaker after thermal reduction at different temperatures which confirms a successful thermal reduction. The reported FTIR results from a published study [22] also showed clear removal for the majority of oxygen functional groups after exposing GO to 800 °C in N₂ atmosphere for 1.0 h and heating rate of 5.0 °C min⁻¹.

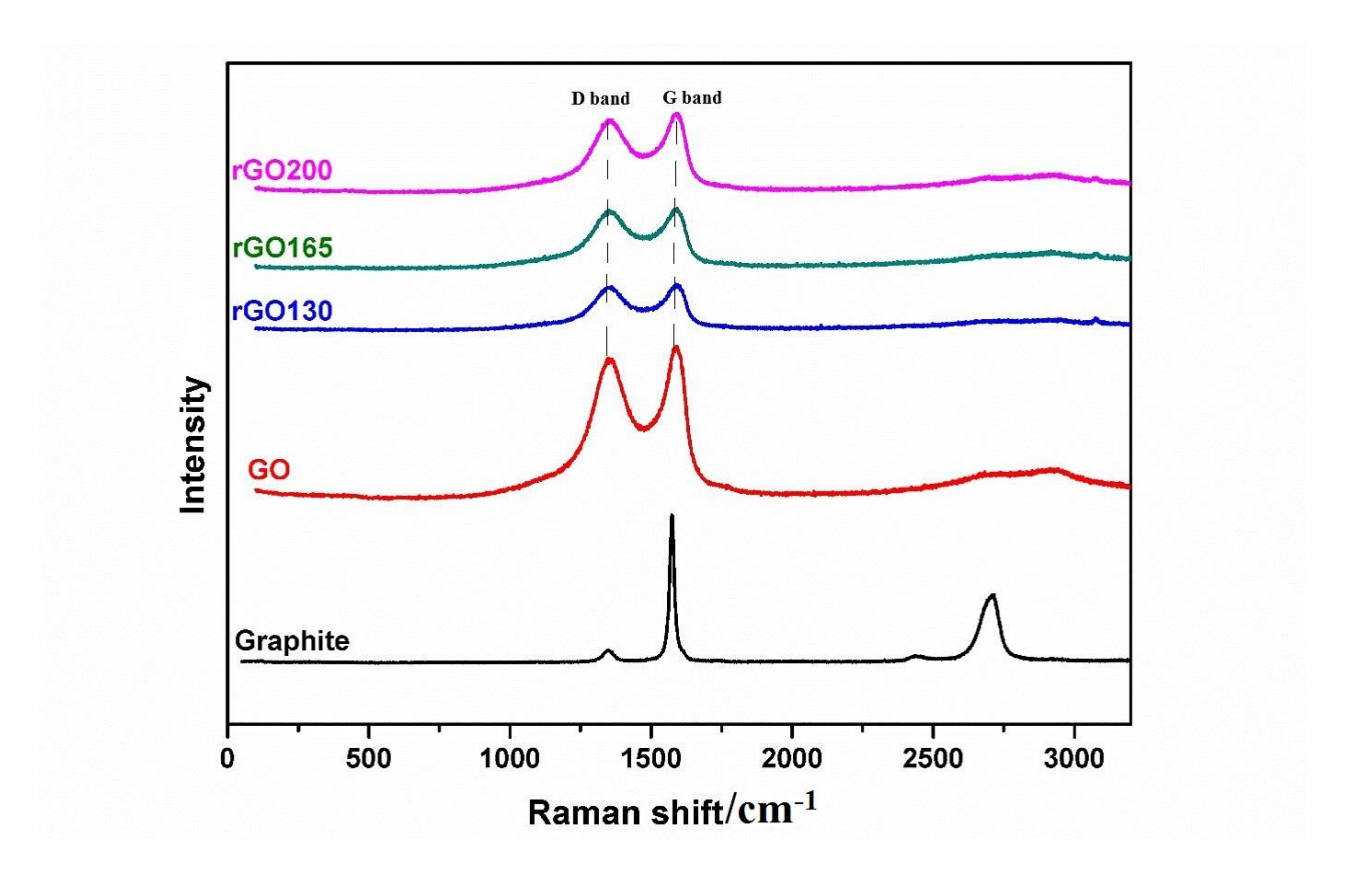


Fig. 2 Raman spectra for graphite, GO and rGOs reduced under different temperatures in a vacuum oven. Spectra have been shifted vertically for clarity

Raman spectroscopy was used to characterize the structure of graphite, and its derivatives GO and rGOs, as shown in Figure 2 D and G bands can be seen in all Raman spectra. D band is due to the breathing of k point phonons of A_{1g} symmetry, while the G band represents first order scattering of the E_{2g} phonons. The defective disorder of the crystalline graphite and the quality of graphitization are important factors that can be evaluated by finding the ratio between intensities of D and G bands (I_D/I_G) [23, 24]. Here, the D band for graphite is 1350 cm⁻¹, whilst the G band is at 1575 cm⁻¹ which is slightly lower than that reported in a previous work [7]. The D band of GO is at

1357 cm⁻¹ which can be attributed to disorder originating from defects. The G band of GO is at 1589 cm⁻¹ and is correlated to C sp^2 in plane vibration [25, 26]. In the GO, the structure of graphene sheets has been drastically disordered due to the oxidization process. An increase of I_D/I_G from 0.092 for graphite to 0.97 for GO gives clear evidence of oxidization. Similar observations regarding the increment of I_D/I_G for the reduced forms of GO compared to graphite were reported in the literature [4, 13]. All the spectra of rGOs have prominent D and G bands. Compared to GO, there is a slight difference in the positions of D band whilst G band for all rGOs remain at the same position. D band can be found at 1353 cm⁻¹ for all rGOs. This slightly lower shifting can be related to the size of in plane sp² domain and formation of defects in the samples [13]. There is a slight increase in I_D/I_G for all rGOs (0.99) as compared with that of GO (0.97).

Some researchers [27] ascribed this tiny increase to the generation of small graphitic domains after reduction. A reported study [13] showed that I_D/I_G increased from 0.95 for GO to 0.96 for rGO which is similar to the current study. Moreover, some researchers [28] elucidated that these new graphitic domains are smaller in size as compared with those present in GO before reduction, but the number of these domains is higher.

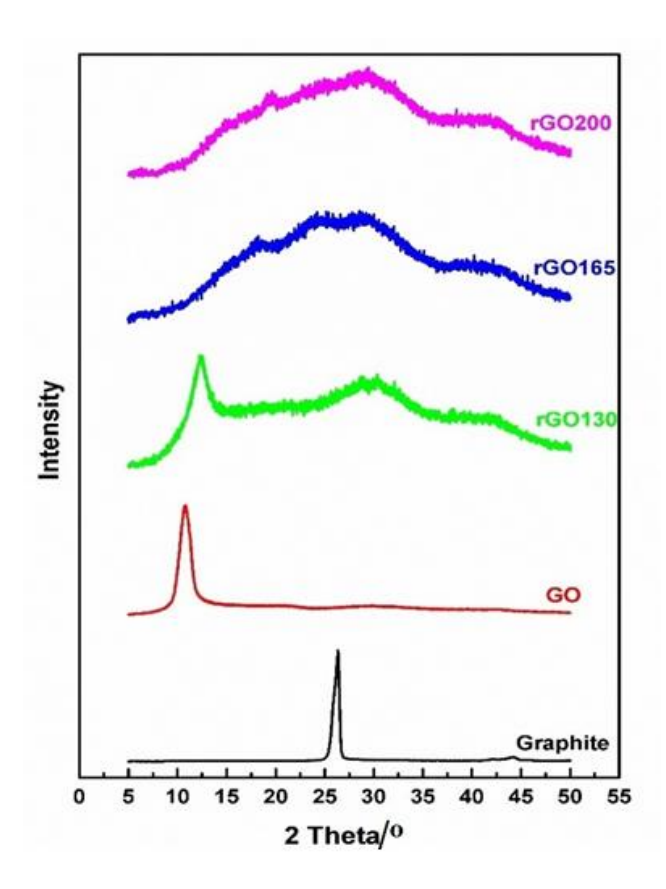


Fig. 3 XRD curves for graphite, GO and rGOs reduced under different temperatures in a vacuum oven. Curves have been shifted vertically for clarity

XRD analysis (Figure 3) demonstrates a sharp peak for pristine graphite at $2\theta = 26.3^{\circ}$, and a wider (001) peak of GO at $2\theta = 10.7^{\circ}$ due to the increased separation of the (001) plane [13]. The interlayer spacing (*d*-spacing) increased from 0.33 nm for pristine graphite to 0.82 nm for GO which can be attributed to the attachment of oxygen functional groups to the (001) plane and edges during the oxidation process [19, 29].

For the rGO, the broad XRD peaks at 2θ 28.8°, 29°, and 29.2° associated with reduced forms of GO obtained at 130, 165, and 200 °C, respectively, are consistent with the reduction of GO to graphene [30]. For rGO130, there is also a relatively intensive peak at $2\theta = 12.3^{\circ}$, corresponding to a d-spacing of 0.73 nm. Two shoulder peaks appeared at $2\theta = 18.3^{\circ}$ and 19.5° for rGO165 and rGO200, indicating smaller *d*-spacing of 0.49 and 0.46 nm, respectively, and higher reduction degrees. The oxidation of graphite leads to a considerable increase in *d*-spacing for GO due to the functionalisation of graphene sheets. Applying reduction by adopting any approach (thermal, chemical, etc.) means the removal of part or all of the functional groups. As a result, depending on the reduction degree rGO may have a similar structure to graphene with corresponding physical characteristics.

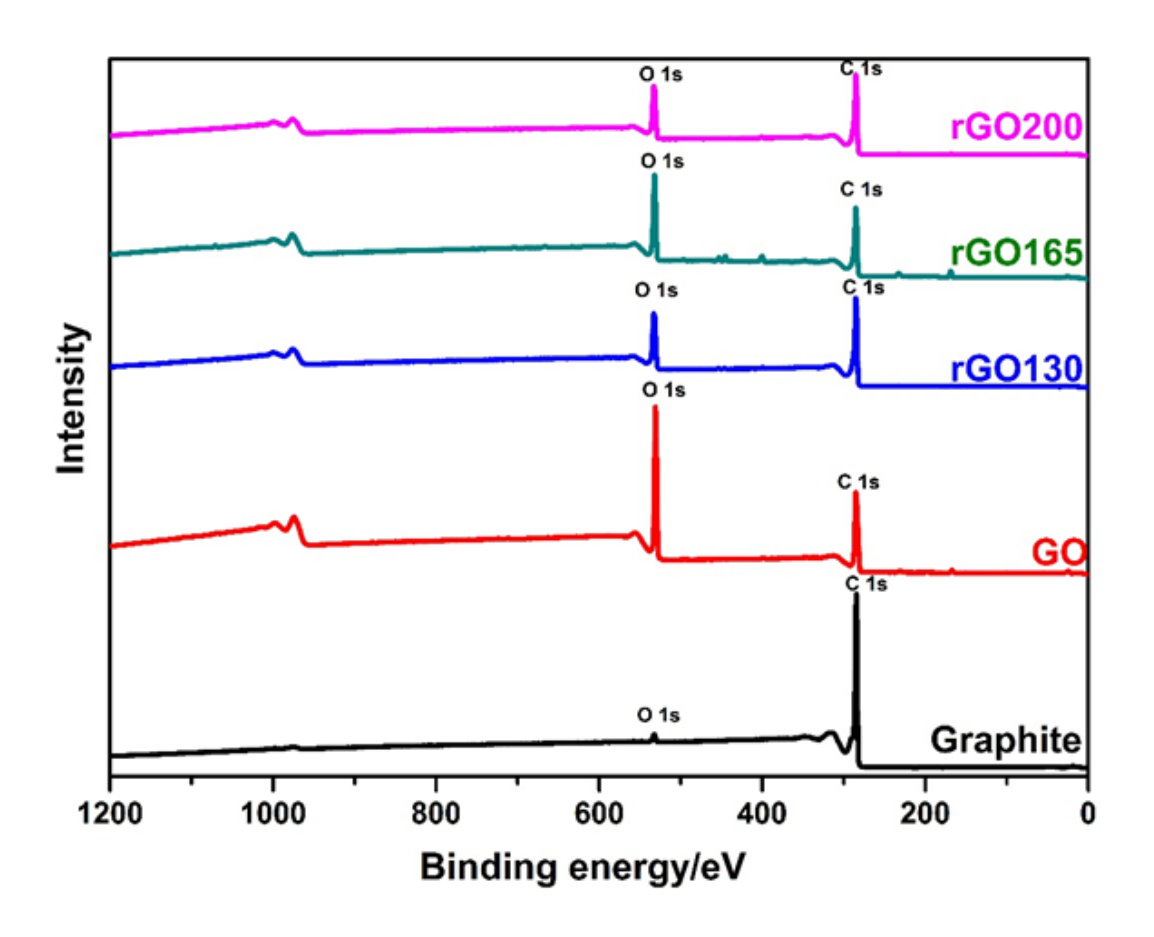


Fig. 4 XPS spectra for graphite, GO and rGOs reduced under different temperatures in a vacuum oven. Curves have been shifted vertically for clarity

XPS was used to examine the chemical composition of the composites. Figure 4 shows the XPS spectra for graphite, GO and rGOs. Table 1 shows the corresponding C and O mass percent, and the calculated C/O mass ratios. The XPS spectrum for graphite shows a tiny peak of O 1s which can be attributed to slight atmospheric oxidation. The sharp peak of C 1s that can be seen for the bare graphite centred at 284.1 eV is due to the Π bond shake up satellite [31]. For the XPS spectrum of GO, it can be clearly seen that the O 1s peak at 540 eV is of significantly higher intensity due to the presence of oxygen containing side groups.

Table 1 Calculated carbon (C) and oxygen (O) mass percentage, and C/O of samples according to XPS

Sample	Graphite	GO	rGO130	rGO165	rGO200
C%	98.39	65.88	67.10	80.90	81.39
Ο%	1.61	31.81	24.87	17.88	17.43
C/O	61.11	2.06	2.69	4.52	4.66

From Table 1, it can be seen that the mass percentage of carbon in the rGO increases with increasing GO reduction temperature, and corresponding mass percentage of oxygen decreases with increasing temperature. As a result, the C/O mass ratio for all rGOs is higher than that for GO confirming a successful thermal reduction. The C/O ratio for GO was found to be 2.06. For the GO reduced at 130 °C, the C/O ratio was 2.69, and the C/O ratios were 4.52 and 4.66 for the GO reduced thermally using 165 and 200 °C, respectively. The C/O ratios after reduction are still significantly higher than that of graphite due to the residual oxygen atoms in graphene sheets. The reduced forms of GO retained some oxygenated functional groups on the surface, in line with the results described above, and these groups might contribute to chemical functionalisation when preparing polymer nanocomposites at the next stage [17, 32]. In figure 5, more details on the components contributing to the C 1_S peaks in the XPS spectra were obtained by NPL software referring to the functional groups in the raw materials, graphite and GO (a and b), and the reduced forms of GO obtained by applying different temperatures (c, d and e). Table 2 shows the binding energy for different functional groups measured from the XPS spectra for graphite, GO and rGOs (Figure 5). For graphite, and as shown in figure 5 (a), the main peak of C=C or C-C relating to sp² and sp³ hybridized species are located at the binding energy of 284.6 eV [33]. Other low intensity peaks can be seen at the binding energies of 286.4 and 288.3 eV due to oxygenated functional groups C-O and O=C-OH respectively [19, 33]. For GO, the contributions of C-O and C=O bonds to the XPS spectrum become much more significant as shown in figure 5(b). The GO spectrum was de-convoluted into C-C or C=C located at 285.0 eV, C-O or carbonyl located at binding energy of 287.1 eV and C=O located at 288.0 eV [14].

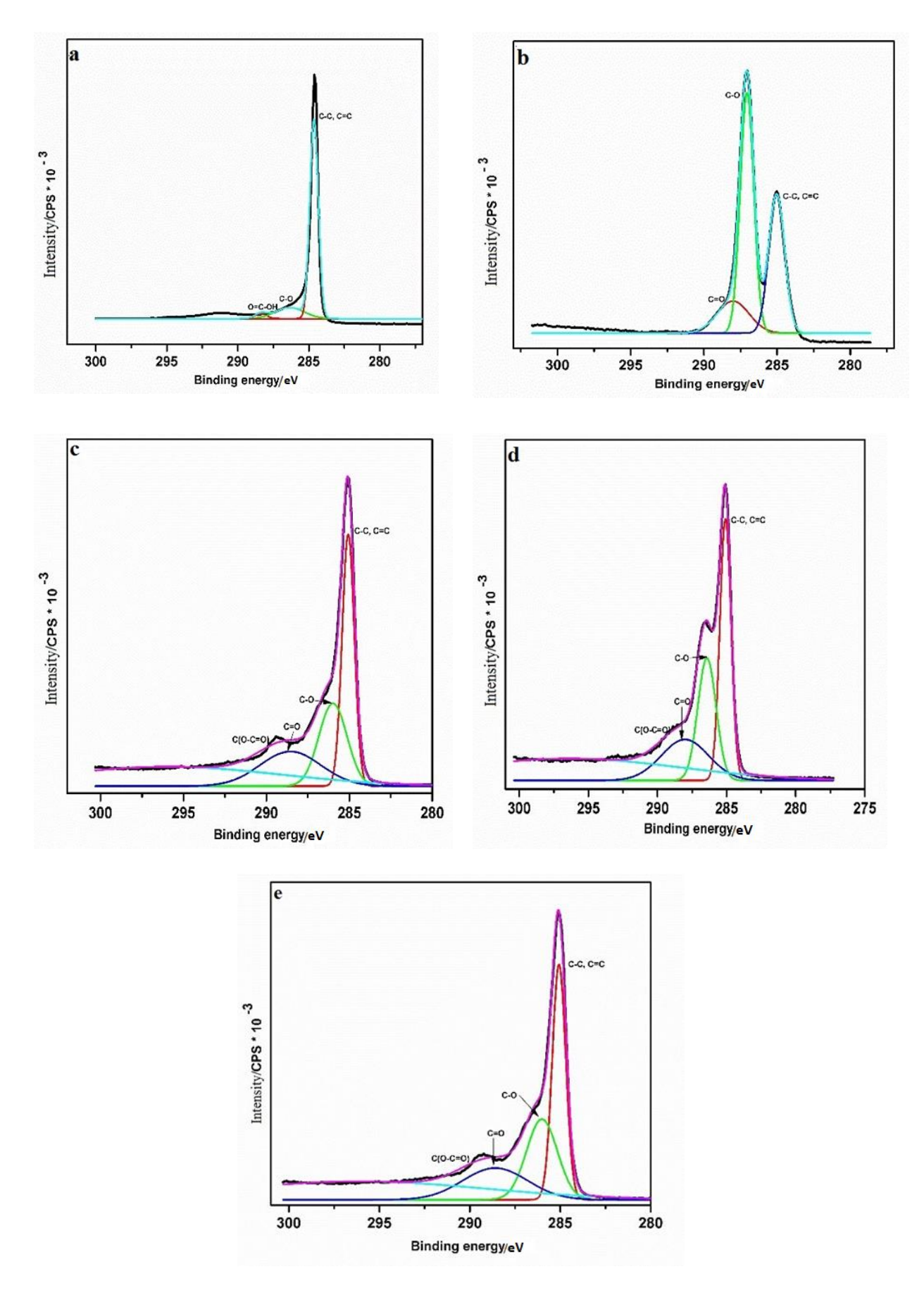


Fig. 5 XPS spectra for (a) graphite, (b) GO, (c) rGO 130, (d) rGO165 and (e) rGO200. Fitting has been carried out to evaluate the components in C 1s from C-C, C=C, C-O, C=O, and C (O-C=O) functional groups

Table 2 The binding energies of functional groups in graphite, GO, and rGOs obtained by XPS

Sample	C-C, C=C/eV	C-O/eV	C=O/eV	COOH/eV
Graphite	284.6	286.4	288.3	288.3
GO	285.0	287.1	288.0	-
rGO 130	285.0	286.0	288.6	290.0
rGO 165	285.1	286.4	288.1	289.4
rGO 200	285.1	286.0	288.5	289.9

As shown in figure 5 (c-e), all the rGOs contained C-O and C=O functional groups as for GO, but the relative intensities of these groups compared to the graphite C-C and C=C groups are lower in the rGOs than for GO. This is attributed to the successful de-oxygenation of the GO using the vacuum assisted low temperature treatment. An additional peak can be seen for the reduced GOs corresponding to the peak of the carboxylic C (O-C=O) group that appears at higher binding energies 289.4 – 290.0 eV. A research group [34] carried out a thermal reduction for GO at 200 °C using hot pressing for a couple of hours following in-situ reduction approach, and obtained a carboxylic group for the reduced form at 289 eV which is similar to this work.

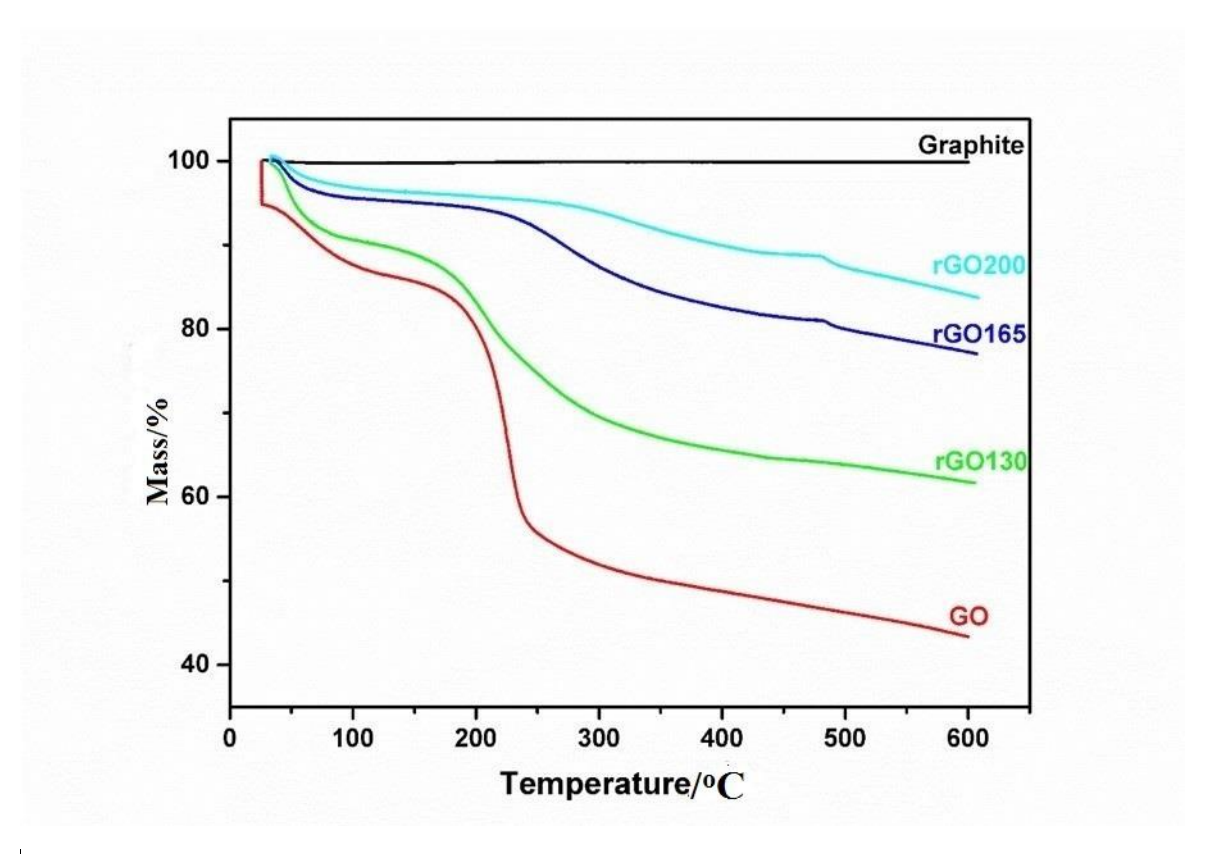


Fig. 6 TGA thermograms for graphite, GO, and reduced graphene oxides rGO130, rGO165, and rGO200

Figure 6 shows the TGA thermograms for graphite, GO, and the three rGOs. From the analysis, graphite has a high thermal stability up to 600 °C (the maximum measurement temperature in this work) due to its highly graphitized structure so there is no mass loss even at a high temperature [16, 32]. By contrast, a significant mass loss is observed for GO between around 200 – 250 °C. The main reason for this loss is the pyrolysis of the unstable oxygen functional groups on the GO surfaces, which is accompanied by emission of gases such as CO, CO₂ and H₂O [32]. GO continuously loses mass after 400°C. The remaining functional groups are more stable, and require higher temperatures to be totally removed [35]. In fact, the mass loss of GO commenced below 100°C, due to adsorbed moisture and experimental setup. Compared to GO, TGA analysis demonstrates that the rGOs are more thermally stable than GO, especially rGO165 and rGO200 from which the majority of the functional groups have been removed by reduction. The rGO130 has a higher mass loss, particularly over the 150 – 300 °C temperature range, due to more remaining oxygen functionalities on the graphene surface and edges after 130 °C reduction.

After TGA heating, the residual mass percentage for GO at 600 °C is 43.5%, compared to 59.3%, 77.0% and 82.9% for rGOs prepared at 130, 165 and 200 °C respectively. This improved thermal stability of rGO compared to GO over the temperature range 25 – 600 °C is consistent with a higher degree of reduction of GO achieved as the reduction temperature under vacuum is increased from 130 °C to 200 °C.

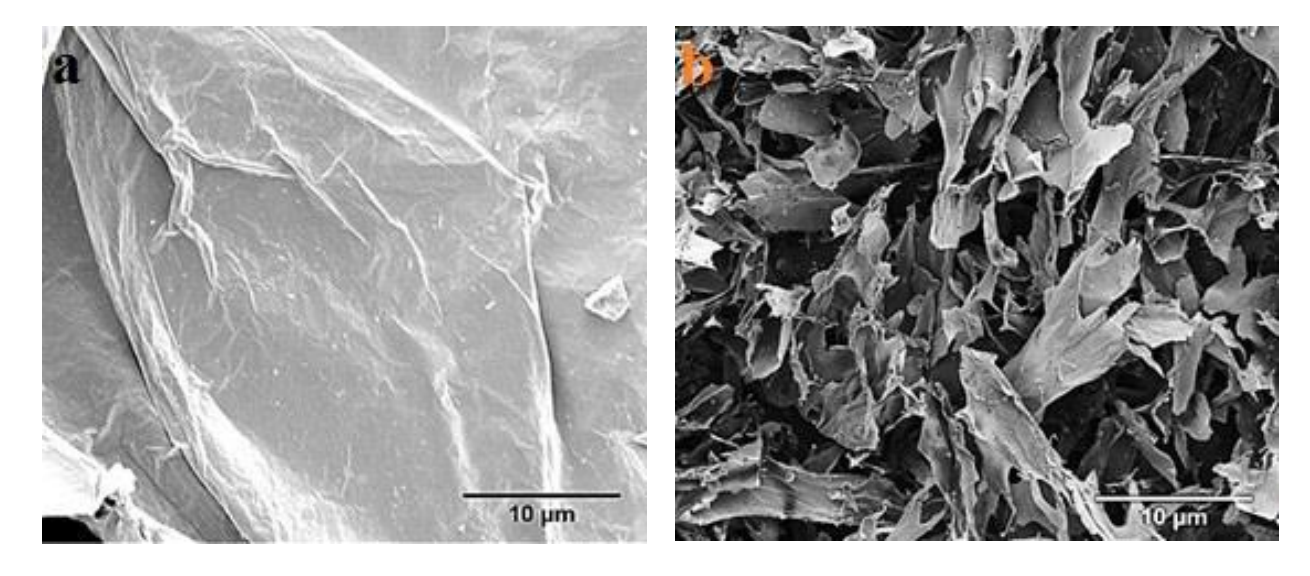


Fig. 7 SEM images of: (a) GO, and (b) rGO130 reduced in vacuum at 130 °C

The microstructure of the GO and rGO materials was examined by low voltage secondary electron imaging in a SEM. Figure 7 a and b shows SEM images for GO and rGO130, respectively. The morphology of the prepared GO (Figure 7a) is a highly exfoliated lamella sheet that has a folded layered structure with obvious wrinkles, and sheet size $> 30 \mu m$. In comparison, the rGO130 consists of markedly smaller $2 - 10 \mu m$ diameter particles in the form of thin sheets with highly irregular edges as shown in (Figure 7 b).

The separate sheet-like rGO particles are crumpled and wrinkled due to van der Waals interactions between the graphene sheets. Following the reduction process, the surface of rGO130 has become rougher compared with the mildly wrinkled morphology of GO. The morphology of the rGO130 surface can be ascribed to the elimination of oxygen functional groups after the process of reduction [36, 37, 7]. The rGO165 and rGO200 exhibited the same sheet-like particle morphology as rGO130.

A research group [35] reported similar crumpled and wrinkled morphology of rGO nano-sheets in an investigation where GO was reduced thermally in a polycarbonate matrix by in situ thermal processing of the nanocomposite at 280 °C.

3.2. PS/rGO nanocomposites

Figure 8 shows the main FTIR peaks of the PS, PS/GO and PS/rGO nanocomposites. Nanocomposites were prepared by mixing PS with 1.0 wt. % of GO, rGO130, rGO165, and rGO200. In the spectrum of PS, the peaks at 698 and 755 cm⁻¹ are related to C-H out of plane bending vibrations of benzene ring, peaks at 902, 1027, 1447, 1491 and 1607 cm⁻¹ are related to the stretching vibration of the benzene ring C=C, peaks at 2920 and 2849 cm⁻¹ are associated with asymmetric and symmetric stretching vibrations of CH₂, and the peak at 3022 cm⁻¹ is related to =C-H aromatic stretching vibration from the benzene ring.

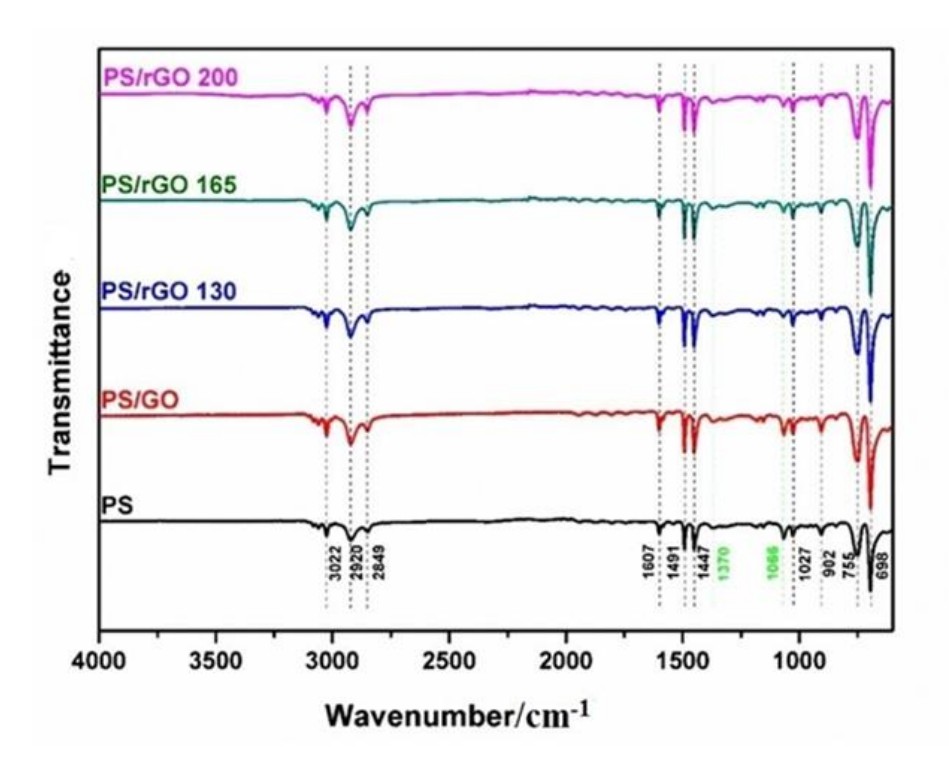


Fig. 8 FTIR spectra of PS, PS/GO, and PS/rGO nanocomposites. The black dash lines refer to the main peaks of PS. The green dash lines refer to peaks associated with possible interactions between PS and GO/rGO

The small FTIR peak at 1370 cm⁻¹, related to –OH, in the spectrum of PS, is seen to increase in intensity in the spectrum of PS/GO, and may be evidence of the presence of GO in the PS [38]. In the spectra of PS/rGO nanocomposites, the main peaks of rGOs shown in figure 1 (mainly C=C and C=O) are undetectable because of their low intensity and/or overlapping of the peaks with the absorption peaks of PS [15].

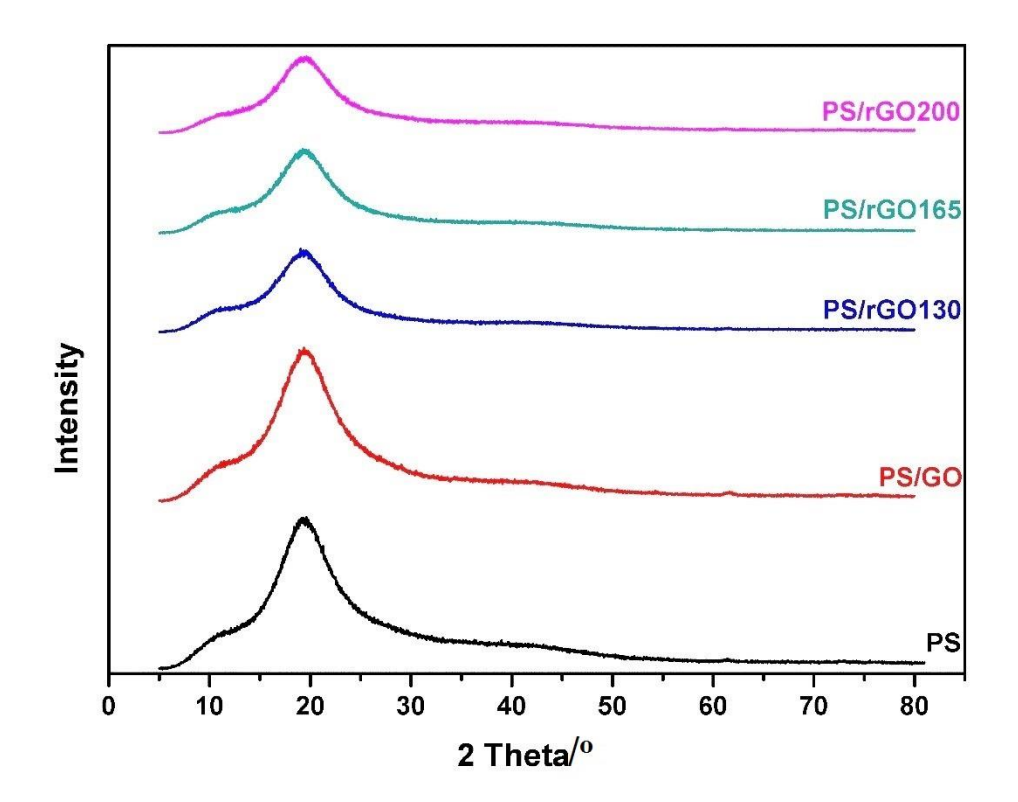


Fig. 9 XRD patterns for PS, PS/GO and PS/rGO reinforced with rGOs reduced under different temperatures in a vacuum oven

Figure 9 depicts the effect of GO and rGOs additions on the XRD patterns of PS nanocomposites. Two main peaks can be seen in the diffraction pattern of PS. The first one at around 10.5° known as "the polymerization peak" can be attributed to the size of the group and the intermolecular backbone-backbone correlation [39]. The second broad peak of PS seen at around 19.3°, is related to the amorphous halo ascribed to the amorphous structure of the PS [40]. The two XRD peaks became weaker in the PS/rGO nanocomposites than those of neat polymer and the PS/GO nanocomposite, attributable to the rGO addition. Due to the low loading of GO and rGO, and the similar peak location of the GO and rGO to that of PS, the peaks of GO and rGO are not identifiable in the XRD curves of their PS nanocomposites. This is consistent with that reported for PS reinforced with holey reduced graphene oxide [39] and PMMA reinforced with rGO [36].

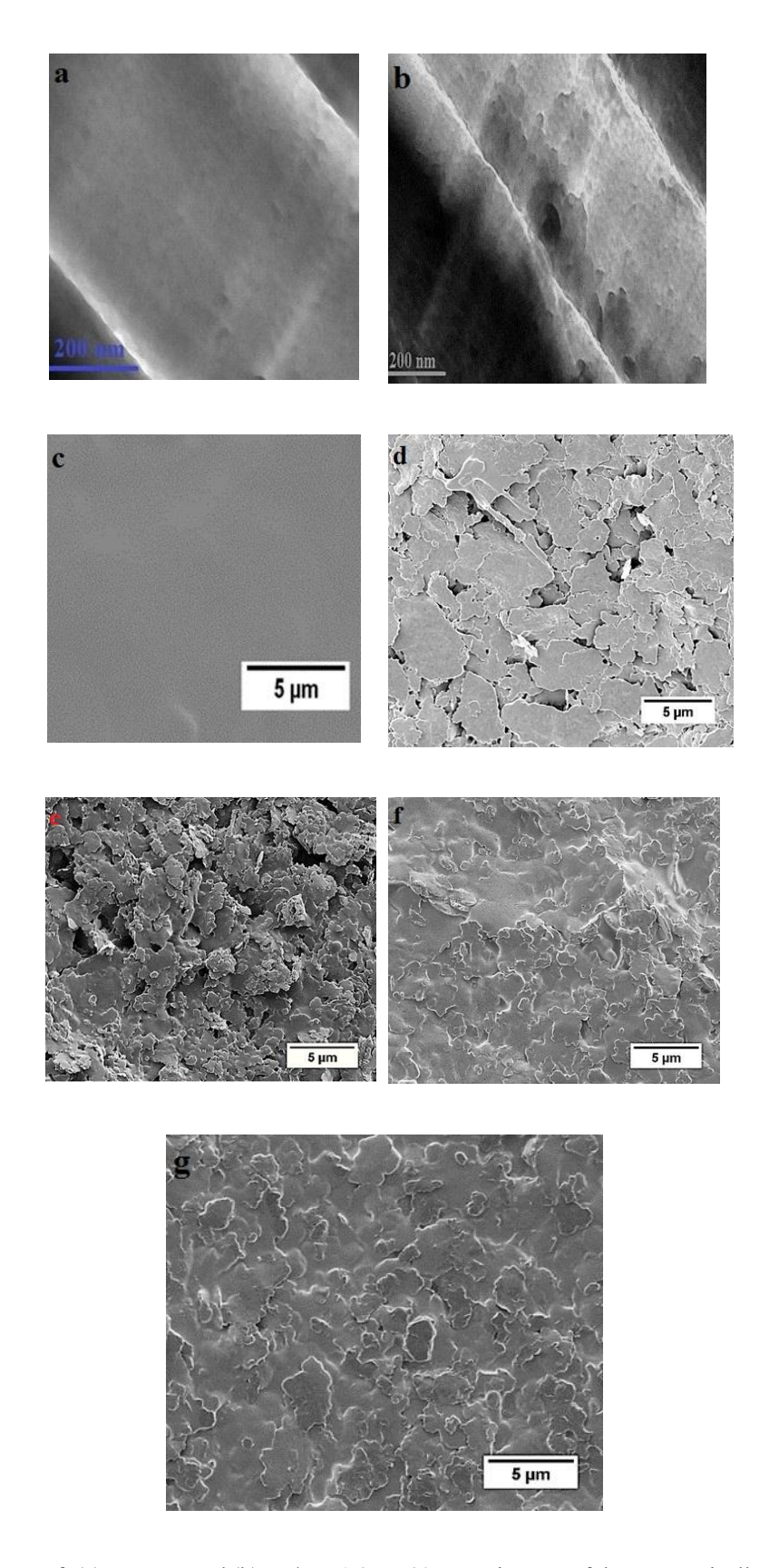


Fig. 10 TEM images of: (a) neat PS, and (b) PS/GO 1.0 wt. %. SEM images of the cryogenically fractured surface of: (c) neat PS, (d) PS/GO, (e) PS/rGO130, (f) PS/rGO165, and (g) PS/rGO200

Figure 10 a and b shows TEM images of PS and PS/GO 1.0 wt. %, whilst Figure 10 c-g are SEM images for the cryogenically fractured surfaces of PS, PS/GO and PS/rGOs. The neat polymer shows no recognizable morphology related to nano-fillers (Figure 10a). On the other hand, curved and partially peeled nano-sheets of GO are finely dispersed in the PS with hardly any aggregation as shown in Figure 10b, suggesting a good dispersion [26]. Figure 10c and d refers to cryogenically fractured surfaces of PS and PS/GO 1.0 wt. %, respectively. Figure 10c appears to have no specific microstructure [21].

It can be seen from figure 10d that the cryogenically fractured surface of PS/GO 1.0 wt. % shows sheet-like features with irregular flakes due to the presence of GO sheets. Generally, the comparison between the cryogenically fractured surface of the pristine PS and PS reinforced with GO and rGOs shows that the latter have rougher surfaces. A research group [24], who employed a thermal reduction process, reported the same surface roughness observation from SEM images of pristine polyvinylidene fluoride (PVDF) compared with PVDF/rGO. The rGO130 nano-sheets (image e) are adhered to PS, with some stacks of sheets in random positions. These stacks of sheets are not clearly seen in the PS/rGO165 (image f) and the PS/rGO 200 (image g), presumably due to better adhesion in these two samples than in the PS/rGO sample. The decreased oxygenated functional groups in PS/rGO165 and PS/rGO 200, caused by thermal reduction at higher temperatures, increased the π - π interaction between the graphene nano-sheets and PS [15].

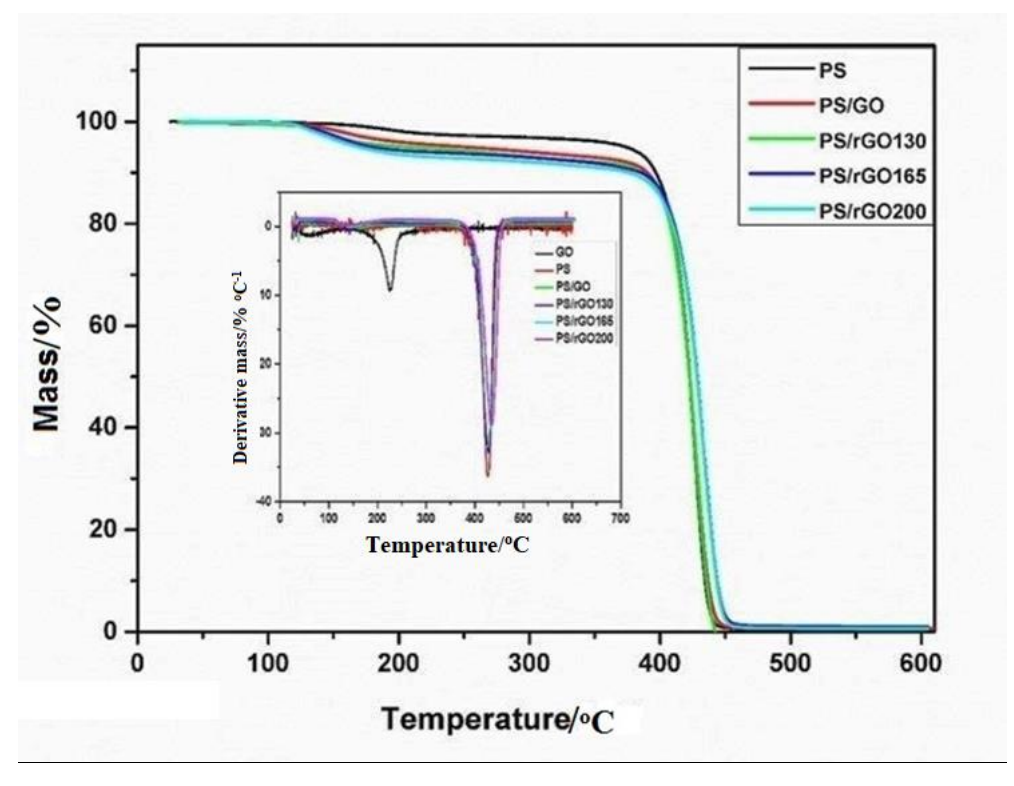


Fig. 11 TGA traces for PS, PS/GO and PS/rGO nanocomposites, with DTG curves for the samples together with GO

Figure 11 shows the TGA traces of PS, PS/GO, and PS/rGO nanocomposites and derivative thermogravimetric (DTG) curves for these samples together with GO. The onset thermal degradation temperature, T_d^{onset} , determined from the TGA curves, for PS is lower than the values for the nanocomposites with GO and rGOs. It increases as the reduction temperature goes higher, indicating improved thermal stability for the nanocomposites. The peak thermal degradation temperature, T_d^{peak} , determined from the DTG curves, of PS is 426.8 °C, similar to what was previously reported [19]. The T_d^{peak} of PS becomes 427.4 °C after the incorporation of GO. This temperature is further improved with the incorporation of rGOs in the matrix to 428.2, 433.3 and 435.1 °C for the nanocomposites of GO reduced using temperatures of 130, 165 and 200 °C, respectively.

A higher thermal reduction temperature leads to an improvement in T_d^{peak} for the nanocomposites compared to the neat polymer. The higher T_d^{peak} can be ascribed to the strong interfacial interaction between the nano-sheets and the matrix. The barrier effect of the nano-sheets, in both the pristine and reduced GOs, may also play a crucial role in inhibiting the heat and diffusion of low molecular mass produced by thermal degradation [41, 42].

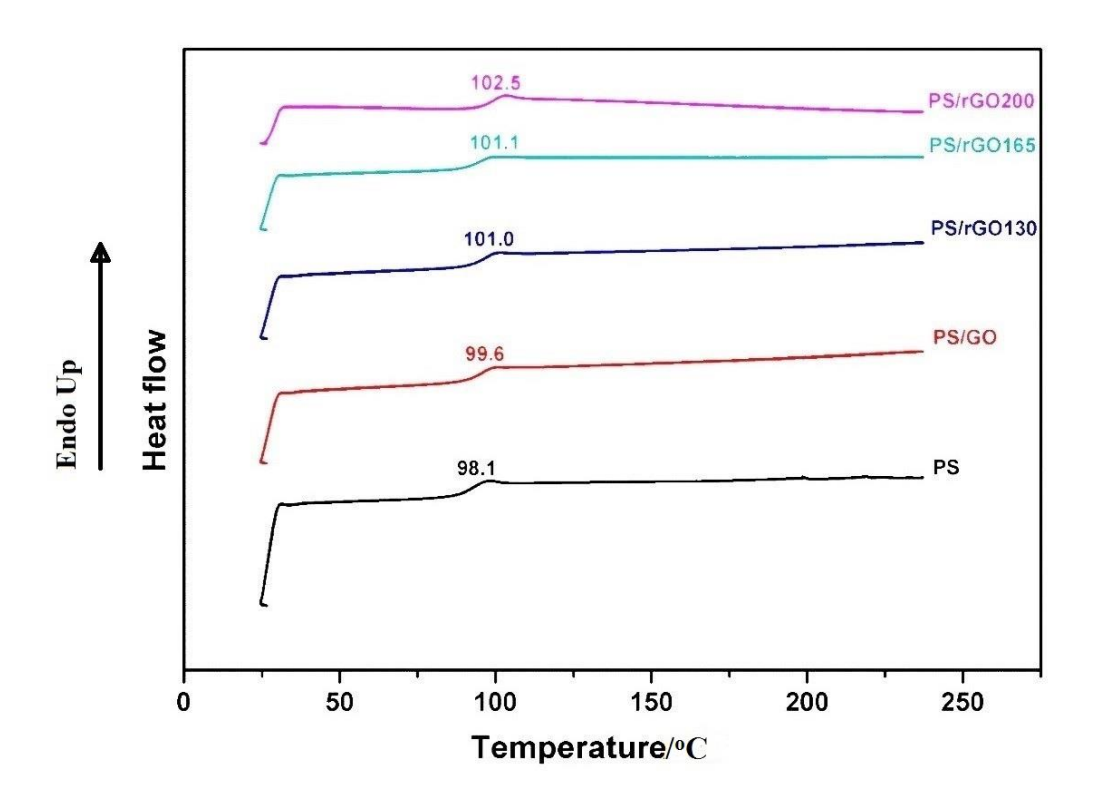
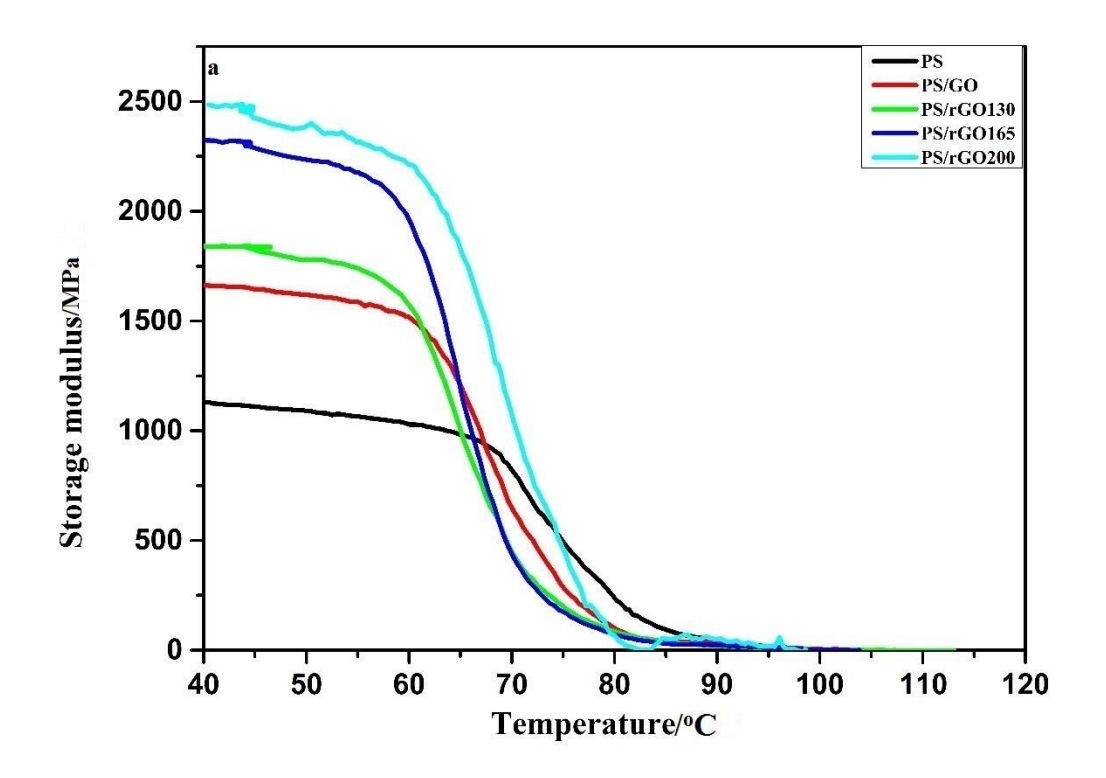
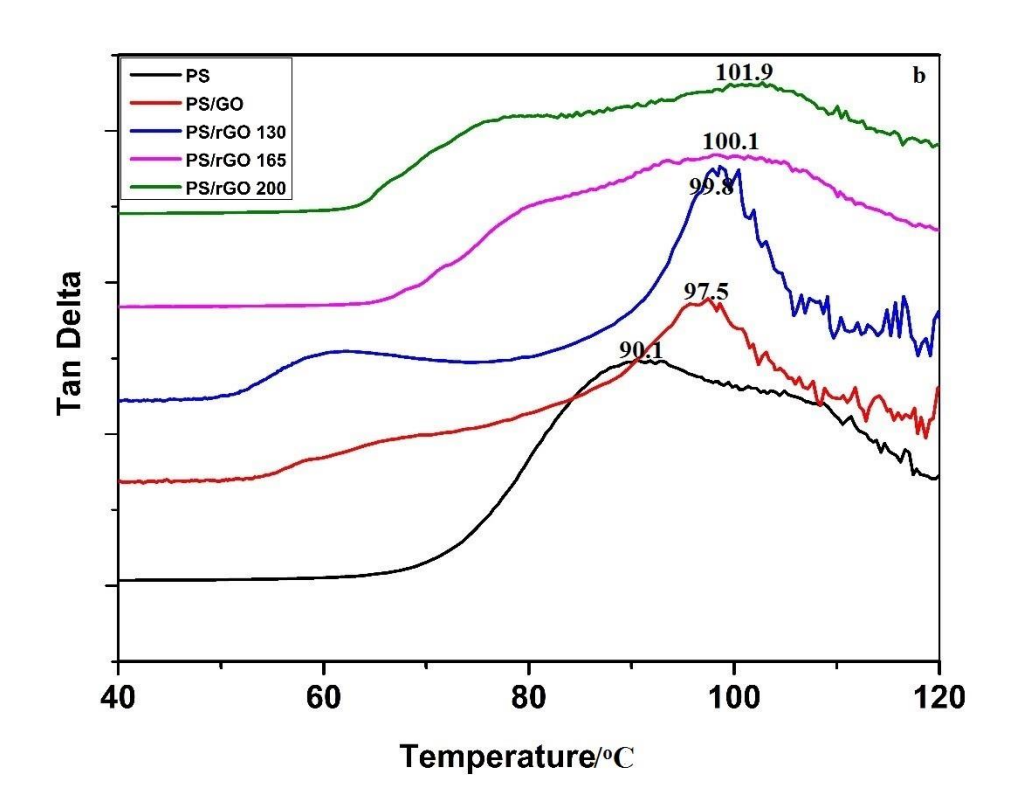


Fig. 12 DSC curves of for PS, PS/GO and PS/rGO nanocomposites

In Figure 12, glass transition temperature, T_g , obtained by DSC can be shown for the polymer and the nanocomposites. T_g is higher for the nanocomposite of PS/GO (99.6 °C) compared with PS (98.1 °C) and more so for the PS reinforced with rGOs. There is a trend of higher T_g for a higher temperature of reduction from 101.0 to 102.5 °C. Similar observations were reported in the literature by other researchers [15] who attributed this increasing T_g trend to the significant effect of the rGO nano-sheets on the restriction of the motion of polymer chains. Higher T_g values confirm the strong interfacial interaction between the polymer matrix and the nano-sheets described above [14, 35, 43].





 $\begin{tabular}{ll} \textbf{Fig. 13} (a) Storage modulus and (b) loss factor versus temperature curves from DMA for PS, PS/GO and PS/rGOs \\ \end{tabular}$

Figure 13 shows the thermomechanical behaviour for the neat polymer, PS with GO and PS reinforced with rGOs. Storage modulus is the elastic response upon the action of deformation. There is a significant increase in the values of this parameter for the nanocomposites that include GO and rGOs compared with the pristine polymer from 1.1 to 2.4 GPa at 40 °C (Figure 13a). The considerable increase in the values of storage modulus can be attributed to the high modulus and a good dispersion of the GO in its pristine and reduced forms in the matrix [15]. Similarly, some researchers [35] found the storage modulus of polycarbonate exhibited a gradual increase with increasing mass fraction of rGO. Figure 13b shows the loss factor (Tan δ) versus temperature curves for the materials. *Tan* δ is an indicator for energy dissipation or damping of the material. It increases in the nanocomposites and with higher reduction degree, attributable to the increasing intermolecular friction in the presence of GO or rGOs. T_g , determined at the peak position of the curves, goes higher as the reduction temperature increases, and T_g for nanocomposites is higher than that of the neat polymer. The trend of T_g , measured by DMA, is the same as by DSC. As described above, the enhancement in T_g is ascribed to the strong interfacial interaction between the nanofillers and the polymer matrix, and the restriction in the movement of polymer chain segments [21, 44]. Table 3 gives a summary of the values of T_d^{prast} , T_d^{peak} , T_g obtained by both DSC and DMA, and storage modulus for the neat polymer, and the nanocomposites.

Table 3 Summary of thermal and thermo-mechanical properties for PS, PS/GO and PS/rGO nanocomposites.

Sample	T _d onset/oC	Tapeak/oC	Tg (DSC)/°C	Tg (DMA)/°C	Storage modulus
					at 40 °C/GPa
PS	380.9	426.8	98.1	90.1	1.1
PS/GO	385.1	427.4	99.6	97.5	1.6
PS/rGO 130	397.8	428.2	101	99.8	1.8
PS/rGO 165	402.1	433.3	101.1	100.1	2.3
PS/rGO 200	404.9	435.1	102.5	101.9	2.4

4. Conclusions

A graphene like material was obtained under the influence of vacuum and low temperatures, which was a greener

approach compared with techniques involving hazardous chemical reductants that generate highly reactive species

with high toxicity and techniques involving the use of much higher heat treatment temperatures. Successful

reduction for GO was obtained for all the low temperatures employed in this study that were 130, 165, and 200

°C. The reduction was confirmed by several techniques of FTIR, Raman spectroscopy, XPS, XRD, and TGA. GO

and its reduced forms were embedded in PS and a range of characterization was carried out for the prepared

nanocomposites. The outcome of the study revealed an improvement in the thermal and thermo-mechanical

properties for the nanocomposites compared with the neat polymer. The polymer nanocomposites that were made

of the reduced forms of GO showed better performance compared to the nanocomposite of the neat polymer and

the pristine GO. The reduced form of GO obtained by the highest reducing temperature of 200 °C showed high

performance in terms of thermal and thermo-mechanical parameters including T_g , T_d^{onset} , T_d^{peak} , and storage

modulus. The prepared nanocomposites by the aforementioned green approach may find potential applications in

supercapacitors, electronics, fire retardance, and automotive.

Acknowledgments

Zaid G. Mohammadsalih would like to express his gratitude for The Ministry of Higher Education and Scientific

Research MOHESR at The Republic of Iraq, The Iraqi Cultural Attaché in London, as well as College of Applied

Science, University of Technology- Iraq, for their moral and financial support for this research. He would also

like to thank Faculty of Engineering at Universiti Putra Malaysia UPM, and Prof. IR. DR. Mohammad Sapuan

Bin Salit for the kind and professional providence of academic resources.

Authors' Contributions

Zaid G. Mohammadsalih: Conceptualization, Methodology, Performing Experiments, Data Analysis, Writing

the original draft, and Editing.

Beverley J. Inkson: Supervision, Reviewing, and Editing.

22

Bigiong Chen: Conceptualization, Methodology, Supervision, Resources, Writing, Reviewing, and Editing.

Declarations

The authors declare that they have no known competing financial interests or personal relationships that could have appeared to influence the work reported in this paper.

References

- [1] Mohammadsalih ZG, Inkson BJ, and Chen B. Structure and Properties of Polystyrene-Co-Acrylonitrile/ Graphene Oxide Nanocomposites. *J. Compos. Sci.* 2023; 7:1-10. DOI: 10.3390/jcs7060225.
- [2] Nethravathi C, Rajamathi M. Chemically modified graphene sheets produced by the solvothermal reduction of colloidal dispersions of graphite oxide. *Carbon* 2008; 46: 1994-1998. DOI: 10.1016/j.carbon.2008.08.013.
- [3] Zhang T, Zhang D, Shen M. A low-cost method for preliminary separation of reduced graphene oxide nanosheets. *Mater. Lett.* 2009; 63: 2051-2054. DOI:10.1016/j.matlet.2009.06.050.
- [4] Ma Q, Song J, Jin C, Li Z, Liu J, Meng S. Zhao J, Guo Y. A rapid and easy approach for the reduction of graphene oxide by formamidinesulfinic acid. *Carbon* 2013; 54:36–41. DOI: 10.1016/j.carbon.2012.10.067.
- [5] Maheshkumar KV, Krishnamurthy K, Sathishkumar K. Sahoo S, Uddin E, Pal SK, Rajasekar R. Research updates on Graphene oxide based polymeric nanocomposites *Polym. Compos.* 2014; 35: 2297-2310. DOI: 10.1002/pc.22899.
- [6] Pei S & Cheng HM. The reduction of graphene oxide. *Carbon*. 2012: 50(9): 3210–3228. DOI: 10.1016/j.carbon.2011.11.010.
- [7] Mohan VB, Brown R, Jayaraman K, Bhattacharyya D. Characterization of reduced graphene oxide: Effects of reduction variables on electrical conductivity. *Mater. Sci. Eng. B.* 2015; 193(B): 49–60. DOI: 10.1016/j.mseb.2014.11.002.
- [8] Toselli M, Fabiani D, Mancinelli P, Frechette M, Heid T, David E, Saccani A. In situ thermal reduction of graphene oxide forming epoxy nanocomposites and their dielectric properties. *Polym. Compos.* 2015; 36: 294–301. DOI: 10.1002/pc.22943.
- [9] Muda MR, Ramli MM, Isa SSM, Jamlos MF, Murad SAZ, Norhanisah Z, Isa MM, Kasjoo SR, Ahmad N, Nor NIM, and Khalid N. Fundamental study of reduction graphene oxide by sodium borohydride for gas sensor application. *AIP Conf. Proc.* 2017; 1808: 1–7. DOI: 10.1063/1.4975267.
- [10] Chua CK & Pumera M. The reduction of graphene oxide with hydrazine: elucidating its reductive capability based on a reaction-model approach. *Chem. Commun.* 2016; 52: 72–75. DOI: 10.1039/c5cc08170j.
- [11] Chen W, Yan L, and Bangal PR. Chemical Reduction of Graphene Oxide to Graphene by Sulfur-Containing Compounds. *J.Phys. Chem. C.* 2010; 114: 19885–19890. DOI: 10.1021/jp107131v.
- [12] Glover, Cai M, Overdeep KR, Kranbuehl DE, and Schniepp HC. In situ reduction of graphene oxide in polymers. *Macromolecules*. 2011; 44: 9821–9829. DOI: 10.1021/ma2008783.

- [13] Chen W, Yan L, Bangal PR. Preparation of graphene by the rapid and mild thermal reduction of graphene oxide induced by microwaves. *Carbon*. 2010; 48: 1146–1152. DOI: 10.1016/j.carbon.2009.11.037.
- [14] Sheng X, Xie D, Cai W, Zhang X, Zhong L, and Zhang H. In situ thermal reduction of graphene nanosheets based poly (methyl methacrylate) nanocomposites with effective reinforcements. *Ind. Eng. Chem. Res.* 2015; 54: 649–658. DOI: 10.1021/ie5035978.
- [15] Han Y, Wang T, Gao X, Li T, Zhang Q. Preparation of thermally reduced graphene oxide and the influence of its reduction temperature on the thermal, mechanical, flame retardant performances of PS nanocomposites. *Compos. A.* 2016; 84(A): 336–343. DOI: 10.1016/j.compositesa.2016.02.007.
- [16] Sharmila BTK, Nair AB, Abraham BT, Beegum PMS, Thachil ET. Microwave exfoliated reduced graphene oxide epoxy nanocomposites for high performance applications. *Polym.* 2014; 55: 3614–3627. DOI: 10.1016/j.polymer.2014.05.032.
- [17] Zhang HB, Wang JW, Yan Q, Zheng WG, Chen C, and Yu ZZ. Vacuum-assisted synthesis of graphene from thermal exfoliation and reduction of graphite oxide. *J. Mater. Chem.* 2011; 21: 5392–5397. DOI: 10.1039/C1JM10099H.
- [18] Qiu S, Hu W, Yu B, Yuan B, Zhu Y, Jiang S, Wang B, Song L, and Hu Y. Effect of functionalized graphene oxide with organophosphorus oligomer on the thermal and mechanical properties and fire safety of polystyrene. *Ind. Eng. Chem. Res.* 2015; 54: 3309–3319. DOI: 10.1021/ie504511f.
- [19] Wu N, She X, Yang D, Wu X, Su F and Chen Y. Synthesis of network reduced graphene oxide in polystyrene matrix by a two-step reduction method for superior conductivity of the composite. *J. Mater. Chem.* 2012; 22: 17254–17261. DOI: 10.1039/C2JM33114D.
- [20] Marcano DC, Kosynkin DV, Berlin JM, Sinitskii A, Sun Z, Slesarev A, Alemany LB, Lu W, and Tour JM. Improved Synthesis of Graphene Oxide. *ACS Nano*. 2010; 4: 4806–4814. DOI: 10.1021/nn1006368.
- [21] Mohammadsalih ZG, Inkson BJ, and Chen B. The effect of dispersion condition on the structure and Properties of polystyrene/graphene oxide nanocomposites. *J. Polym. Compos.* 2021; 42: 320-328. DOI: 10.1002/pc.25827.
- [22] Ju HM, Huh SH, Choi SH, Lee HL. Structures of thermally and chemically reduced graphene. *Mater. Lett.* 2010; 64: 357-360. DOI: 10.1016/j.matlet.2009.11.016.
- [23] Eda G & Chhowalla M. Chemically derived graphene oxide: Towards large-area thin-film electronics and optoelectronics. *Adv. Mater.* 2010; 22: 2392–2415. DOI: 10.1002/adma.200903689.
- [24] Tang Z, Zhang L, Zeng C, Lina T and Guo B. General route to graphene with liquid-like behavior by non-covalent modification. *Soft Matter*. 2012; 8: 9214–9220. DOI: 10.1039/c2sm26307f.
- [25] Li Y, Umer R, Abdul Samad Y, Zheng L, Liao K. The effect of the ultrasonication pre-treatment of graphene oxide (GO) on the mechanical properties of GO/polyvinyl alcohol composites. *Carbon*. 2013; 55: 321–327. DOI: 10.1016/j.carbon.2012.12.071.
- [26] Mohammadsalih ZG & Sadeq NS. Structure and properties of polystyrene/graphene oxide nanocomposites. *Fuller Nanotub Car N.* 2022; 30: 373-384. DOI: 10.1080/1536383X.2021.1943367.
- [27] Park W, Hu J, Jauregui LA, Ruan X, and Chen YP. Electrical and thermal conductivities of reduced graphene oxide/polystyrene composites. *Appl. Phys. Lett.* 2014; 104: 1-5. DOI: 10.1063/1.4869026.
- [28] Stankovich S, Dikin DA, Piner RD, Kohlhaas KA, Kleinhammes A, Jia Y, Wu Y, Nguyen ST, Ruoff RS. Synthesis of graphene-based nano-sheets via chemical reduction of exfoliated graphite oxide. *Carbon*. 2007; 45: 1558–1565. DOI: 10.1016/j.carbon.2007.02.034.
- [29] Suresh D, Udayabhanu, Nagabhushana H, Sharma SC. Clove extract mediated facile green reduction of graphene oxide, its dye elimination and antioxidant properties. *Mater. Lett.* 2015; 142: 4–6. DOI: 10.1016/j.matlet.2014.11.073.

- [30] Mokhtar MM, Abo El Enein SA, Hassaan MY, Morsy MS, and Khalil MH. Thermally Reduced Graphene Oxide: Synthesis, Structural and Electrical Properties. *Int. J. Nanoparticles Nanotechnol.* 2017; 3: 1–9. DOI: 10.35840/2631-5084/5508.
- [31] Szabo' T, Berkesi O, Forgo' P, Josepovits K, Sanakis Y, Petridis D, and De'ka'ny I. Evolution of surface functional groups in a series of progressively oxidized graphite oxides. *Chem. Mater.* 2006; 18: 2740–2749. DOI: 10.1021/cm060258+.
- [32] Tang LC, Wang X, Gong LX, Peng K, Zhao L, Chen Q, Wu LB, Jiang JX, Lai GQ. Creep and recovery of polystyrene composites filled with graphene additives. *Compos. Sci. Technol.* 2014; 91: 63–70. DOI: 10.1016/j.compscitech.2013.11.028.
- [33] Wollbrink A, Ruscher CH, Volgmann K, Koch J, Breukscha A, Tegenkamp C, Caro J. Improved hydrogen selectivity of Surface Modified Graphite (SMG) membranes: Permeation experiments and characterization by micro-Raman spectroscopy and XPS. *J. Membr. Sci.* 2017; 528: 316–325. DOI: 10.1016/j.memsci.2016.12.067.
- [34] Tang H, Ehlert GJ, Lin Y, and Sodano HA. Highly efficient synthesis of graphene nanocomposites. *Nano Lett.* 2012; 12: 84–90. DOI: 10.1021/nl203023k.
- [35] Xu C, Gao J, Xiu H, Li H, Zhang J, Luo F, Zhang Q, Chen F, Fu Q. Can in situ thermal reduction be a green and efficient way in the fabrication of electrically conductive polymer/reduced graphene oxide nanocomposites? *Compos. A.* 2013; 53(A): 24–33. DOI: 10.1016/j.compositesa.2013.06.007.
- [36] Tripathi SN, Saini P, Gupta D, Choudhary V. Electrical and mechanical properties of PMMA/reduced graphene oxide nanocomposites prepared via in situ polymerization. *J. Mater. Sci.* 2013; 48: 6223–6232. DOI 10.1007/s10853-013-7420-8.
- [37] Saravanan N, Rajasekar R, Mahalakshmi S, Sathishkumar TP, Sasikumar KSK, and Sahoo S. Graphene and modified graphene-based polymer nanocomposites A review. *J. Reinf. Plast. Compos.* 2014; 33: 1158–1170. DOI: 10.1177/0731684414524847.
- [38] Wan C & Chen B. Reinforcement and interphase of polymer/graphene oxide nanocomposites. *J. Mater. Chem.* 2012; 22: 3637–3646. DOI: 10.1039/c2jm15062j.
- [39] Aldawsari Y, Mussa Y, Ahmed F, Arsalan M, and Alsharaeh E. Novel Synthesis of Holey Reduced Graphene Oxide / Polystyrene (HRGO/PS) Nanocomposites by Microwave Irradiation as Anode for High-Temperature Lithium-Ion Batteries. *Materials* 2019; 12: 2248 (1–14). DOI: 10.3390/ma12142248.
- [40] Han Y, Wu Y, Shen M, Huang X, Zhu J, Zhang X. Preparation and properties of polystyrene nanocomposites with graphite oxide and graphene as flame-retardants. *J. Mater. Sci.* 2013; 48: 4214–4222. DOI 10.1007/s10853-013-7234-8.
- [41] Yang J, Huang L, Li L, Zhang Y, Chen F, Zhong M. Preparation of polystyrene/graphene oxide composites and their supercritical carbon dioxide foaming. *J. Polym. Res.* 2013; 20: 173 (1–9). DOI 10.1007/s10965-013-0173-x.
- [42] Qiu F, Hao Y, Li X, Wang B, Wang M. Functionalized graphene sheets filled isotactic polypropylene nanocomposites. *Compos. B: Eng.* 2015; 71: 175–183. DOI: 10.1016/j.compositesb.2014.11.027.
- [43] Alsharaeh EH, Othman AA & Aldosari MA. Microwave irradiation effect on the dispersion and thermal stability of RGO nano-sheets within a polystyrene matrix. *Materials* 2014; 7: 5212–5224. Doi: 10.3390/ma7075212.
- [44] Al Ani AZ, Zaidan SA. Statistical Analysis of Mechanical Strength and Dielectric Breakdown of Polyester Nano-Alumina Composites. *J. Appl. Sci. Nanotechnol.* 2023; 3: 1-11. DOI: 10.53293/jasn.2022.4973.1168.